Studies of Forward Neutral Energy in Au-Nucleus Collisions at the AGS

Mark Clemen W. Cleland

October 4, 1996

1 Introduction

The charge of Experiment E814/E877 has been to explore the global event properties of Nucleus-Nucleus collisions at relativistic energies. These are global properties such as energy-flow, initial-state baryons, and final state multiplicity measured over a wide range of rapidity. A broad picture of the collision dynamics has come out of this, resulting in a general picture of heavy ion collisions at these energies. As E877 data-taking has ended with a steady Au beam in a well-understood spectrometer, we endeavored to complete the intent of these experiments as they were begun, studying the fragmentation of the projectile into beam-rapidity nucleons, only now with the Au beam.

A simple though prevalent model divides the initial state baryons in relativistic heavy ion collisions into spectators and participants. The participants in the interaction undergo strong inelastic collision(s), and the spectator nucleons are presumed to be unaffected by the collision. The mean number of forward, beam-rapidity nucleons as a function of some parameter broadly proportional to the number of participants (such as transverse energy) provides an interesting test of the model, and perhaps insight into the first-order scattering dynamics. Such a measurement is also a test of the stopping power of the nucleus, and of the validity of the 'unaffectedness' of the supposed spectators.

There is another, more pragmatic reason for making this measurement in Au-Au collisions at relativistic energies. Upcoming collider experiments at

RHIC require methods for characterizing event structure, globally, and independently of such measurements as transverse energy, such as in a search for chiral symmetry breaking. Unfortunately at RHIC, the prospects for zero-degree calorimetry are constrained by the accelerator magnets themselves, and are limited in fiducial area as well as limited to neutrally-charged particles.

One measurement previously made was by the predecessor to E877, E814 [1]. This was a measurement of the mean number of beam rapidity protons as well as neutrons using a (14.7 GeV/c)/nucleon Silicon beam, incident on Aluminum, Copper and Lead. The results are summarized in Figure [1]. The mean multiplicity of forward baryons is shown as a function of transverse energy in the backward pseudorapidity range of (-0.5, 0.8) in the lab frame. The near symmetric-collision (Si-Al) data show a plateau in the number of beam rapidity baryons at small impact parameter, while the asymmetric system, Si-Pb, shows an exponential dropoff with increasing centrality. This measurement was made using energy-cluster finding in the forward calorimetry, and cutting on beam rapidity energy. Furthermore, the protons were tracked in drift chambers, and matched to the clusters.

2 Measurements

2.1 Analysis Description

The AGS provided a Gold beam with a momentum of 11.7 GeV/c/nucleon. The E877 spectrometer relevant to this measurement is shown in Figure 2. One difficulty with the previous E814 measurement was that the TCAL is hadronically "thin", and suffers added energy fluctuations due to leakage. Further, tracking over a wide range of transverse energy, especially as in Au-Au collisions, is problematic at best. By restricting the measurement to the neutrons as a function of the participant calorimeter (PCAL) transverse energy (covering a pseudorapidity range of (1.0, 4.0) in the lab frame), with no tracking, we expect to minimize the inefficiencies and systematic errors that would otherwise plague the measurement. The neutron region is expected to be clean of other confusing sources, and we can further clean the signal with a scintillator array in front of the calorimeters to get rid of secondary charged particles that bend into this region by the analyzing magnet.

Figure 1: Forward beam-rapidity baryon mean multiplicity as a function of centrality, as measured in E814. Note the different curve shapes for the symmetric and the unsymmetric collisions.

Figure 2: The subset of the 877 spectrometer relevant to this measurement. The active detectors were the BVER, the TOFU scintillators, the Forward Scintillators, and the calorimetry.

The forward calorimeters consist of the calorimeter modules originally designed for ISR experiment 807, and refined and rebuilt for E814 [2] [3] [4]. These consist of layers of scintillator with depleted-uranium absorber, and interspersed with copper. Using the Uranium noise, they are self-calibrating for gain and stability of response. These UCAL's were position 36.3 meters downstream from the target. An analyzing magnet with $\int B \cdot dl$ of 1.95 T-m was positioned at $\approx$ 1m downstream from the target. The TOFU scintillators, the Forward Scintillators, and the TCAL were also read out during this data taking. None of the 877 tracking chambers were read out. Since many of the triggers taken were at higher impact parameters where the spectrometer is flooded with a high multiplicity of secondaries, the tracking chambers were not deemed to be useful. Since many of the data taken were simple beam triggers and time-of-flight was not found to be useful, the gains on the TOFU scintillators were decreased from the usual, by a factor of 5-10.

The data consist of 650k triggers for each of the 4 targets (1.0% nuclear interaction length of Au, 1.9% Au, 2% Al, and 2.1% Cu), plus 650k triggers for the MT target (an empty space in the target holder). This program was performed for zero and full B field ($\approx$ 2 T-m), as well as 1/3 and 2/3 B fields in the analyzing magnet M1. At full strength, the analyzing magnet deflected the beam by $\approx$ 3.5 UCAL stacks from the experiment center line, and the protons by $\approx$ 8 UCAL stacks. The characteristic width of a hadronic shower in the UCAL's is $\approx$ 1 UCAL stack.

At low transverse energy (E_t), the neutron region is heavily contaminated by the tails of the beam shower, as well as collisions in the target holder instead of the target, and upsteam of the target. These effects are taken into account by the MT target subtraction, although at small transverse energies the errors are very large. We restricted the measurement to $\approx 1/2$ of the neutron region, that half on the side of the experiment center line away from the beam. Furthermore, those forward scintillators covering slightly more than this region were summed and a veto of $\approx 2/3$ of a minimum-ionizing signal was made on the sum. Also, events with PCAL E_t and UCAL forward energy together indicative of overlapping beam particles were vetoed. All of the graphs presented here, unless otherwise indicated, are for the fiducial region of the measurement, and are not corrected for geometrical losses. The triggers were a mix of parallel beam-coincidence triggers and TCAL transverse energy triggers.

Shown in Figure 3 (top) are a set of E_t distributions taken with the primary parallel triggers plotted as a function of PCAL E_t (GeV) in one data-taking run, in this case, the data for the thin Au target. The solid curve shows the beam triggers, the next shows the TCAL1 triggers, then TCAL2, then TCAL3 (the highest E_t triggers). The data are downscaled, shown in the top figure are simply the raw statistics from the run per PCAL E_t bin. The bottom curve is corrected for the downscaling, and is normalized to total number of beam particles. The TCAL3 triggers were not downscaled, so that curve does not change. These plots show the classic E_t "plateau", as well as the statistics out to the edge of the fall-off. These bins are 3.5 GeV in PCAL E_t each, there being even at 300 GeV E_t 10 events or so per bin. The final measurement was made in $\approx$7 GeV bins in PCAL E_t.

2.2 Transverse Energy and centerline-UCAL Energy

If one simply calculates the mean PCAL transverse energy as a function of UCAL neutron-region energy for beam triggers, then of course the results depend on the target thickness. For these thin targets, most of the beam particles do not interact strongly in the target, yet produce neutron-region energy by EMD disassociation. One requires some minimum-bias cut on the nuclear interactions measured in the region of the target.

Since we are averaging over the transverse energy in the PCAL, it would not do to cut on this same quantity to define "minimum bias". Instead, the TCAL energy was cut on. These are correlated of course, but the effect of truncating the PCAL E_t spectrum is minimized. Figure 4 shows the dependence of the TCAL energy on PCAL energy. The cut used here was TCAL total energy greater than 2 GeV.

We calculate the mean PCAL transverse energy as a function of UCAL energy observed in the neutron region. The results for the different targets are shown Figures 5, 6, and 7. For the Au target data, Figure 7, (the relevant result for RHIC) one sees that the mean transverse energy is proportional to the center-line neutral energy over a broad range of E_t. This is of course with the understanding that there is some criteria for eliminating "minimum bias" events. The error bars reflect the error on the mean, while the lower curves show the actual widths of the E_t distributions about the mean. The widths are typically small compared to the mean, especially for the more central collisions.

Shown in Figure 8 is the same data for the thin Au target, as well as the

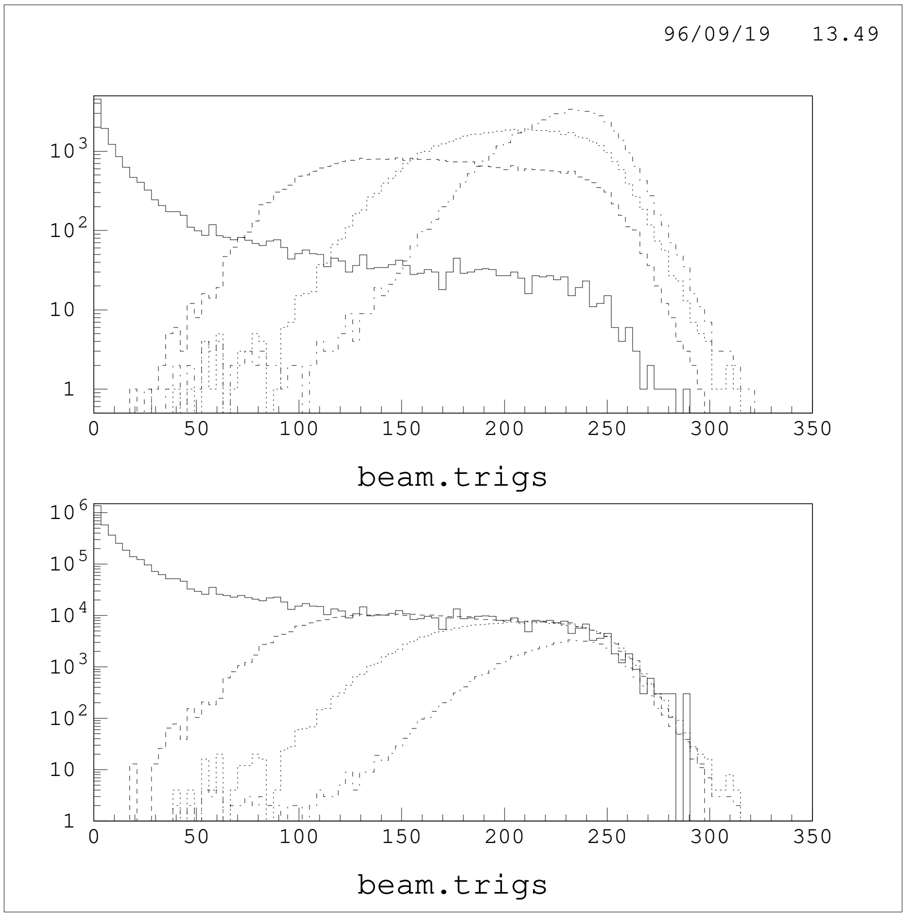

Figure 3: Plots of $\frac{dN}{dE_t}$ taken with different triggers for the thin Au target with full B field, for one data-taking run, as a function of E_t. The top curve shows the raw statistics, the bottom curve is corrected for downscaling. The triggers shown are, from left to right, the beam triggers, and the TCAL1, TCAL2 and TCAL3 energy flow triggers.

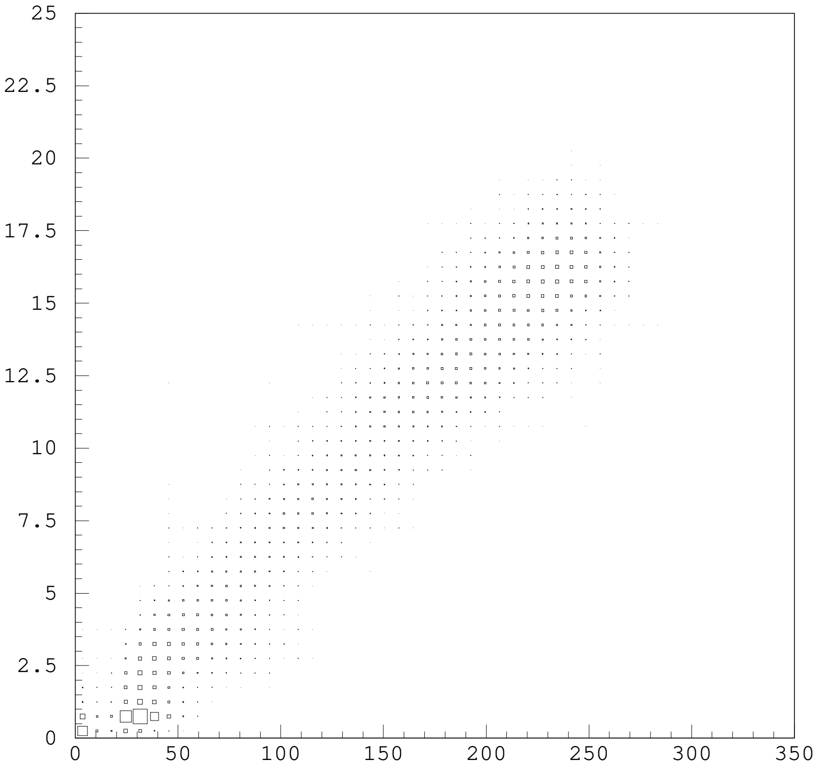

Figure 4: Scatterplot of TCAL total energy against the PCAL transverse energy. The "minimum bias" cut required TCAL energy greater than 2 GeV. Note that most of the data are beam triggers below this cut.

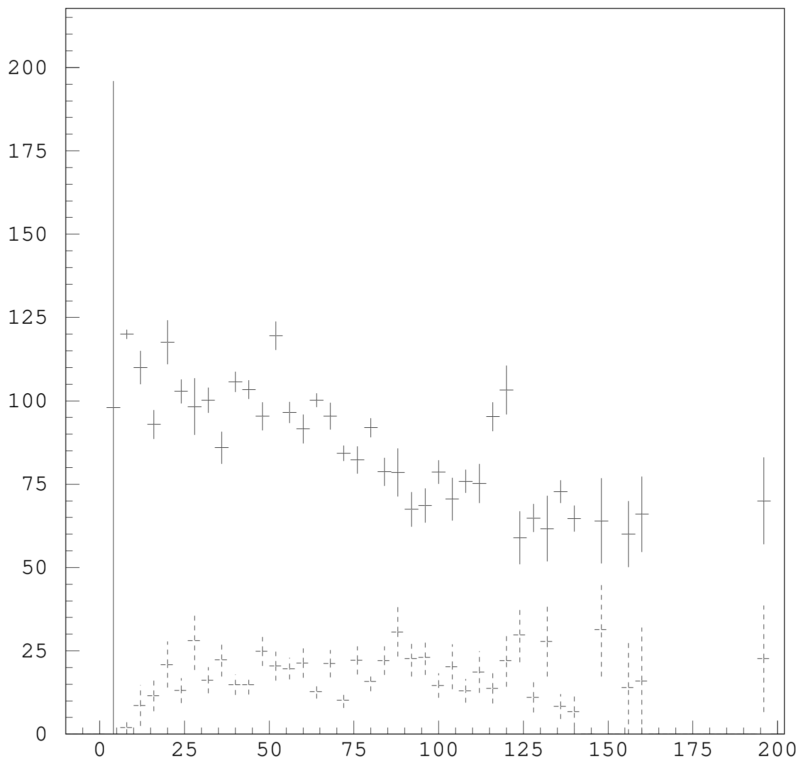

Figure 5: Mean PCAL transverse energy as a function of the forward neutron-area energy for the Au beam incident on the Aluminum target. The mean was formed using a cut on the forward scintillators around the neutron fiducial area, requiring no charge particles, and on the TCAL energy, requiring more than 2 GeV transverse energy in the TCAL. Also shown is the width of the distribution in the lower curve.

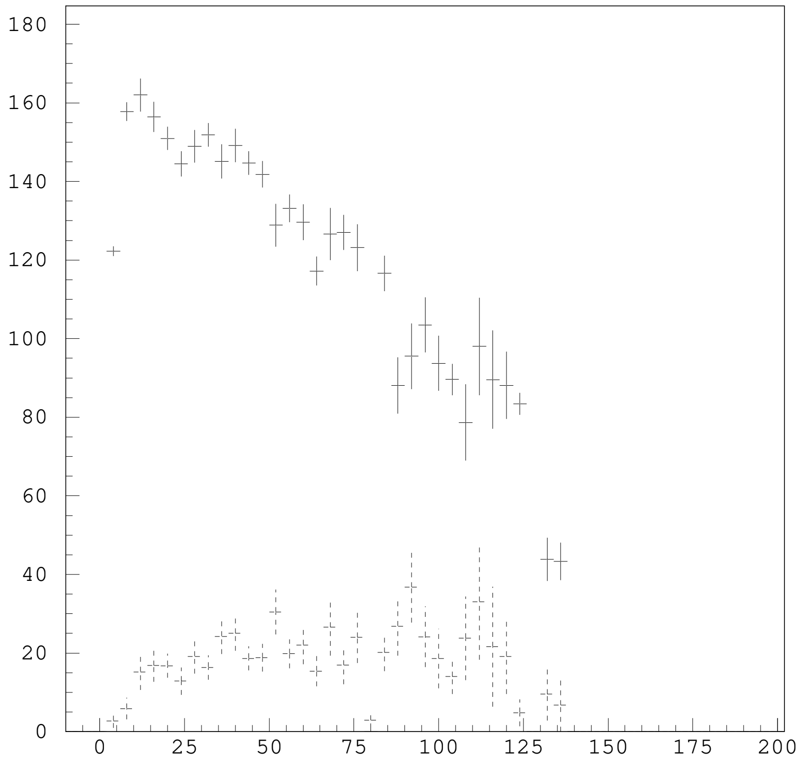

Figure 6: Mean PCAL transverse energy as a function of the forward neutron-area energy for the Au Beam incident on the Copper target. Also shown is the width of the distribution.

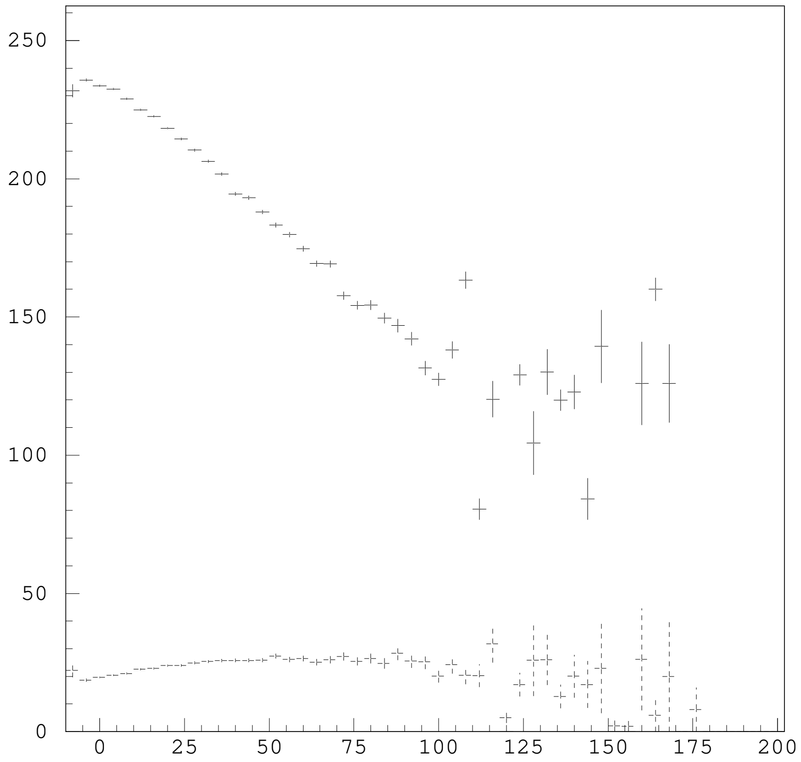

Figure 7: Mean PCAL transverse energy as a function of the forward neutron-area energy for the Au Beam incident on the 1% Gold target. Also shown is the width of the distribution.

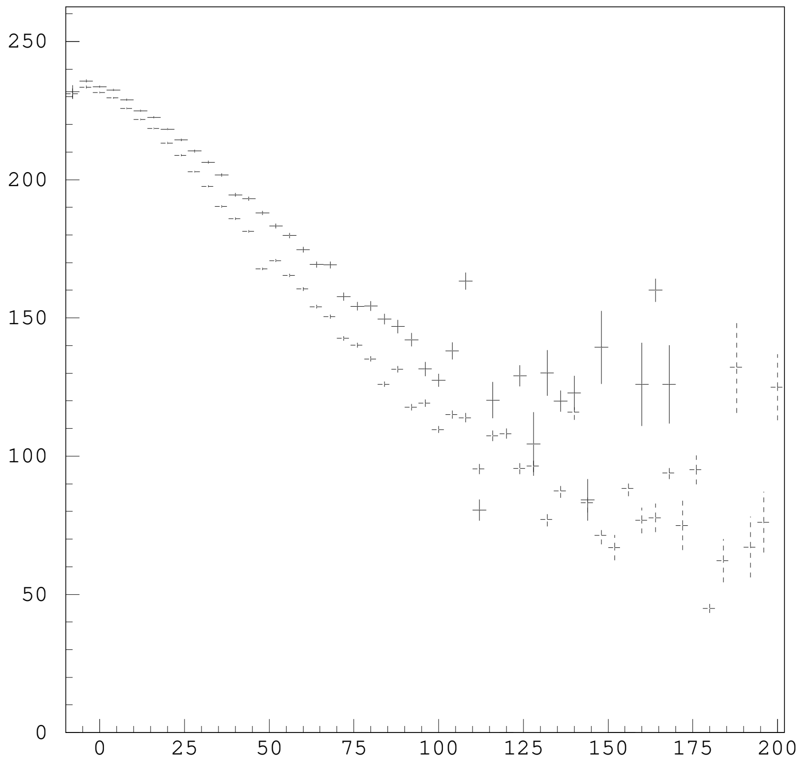

Figure 8: Mean PCAL transverse energy as a function of the forward neutron-area energy for the Au beam incident on the 1% target. The slightly lower (dashed) points are the same, only without the charged particle veto using the forward scintillators in front of the neutral region in the UCALs.

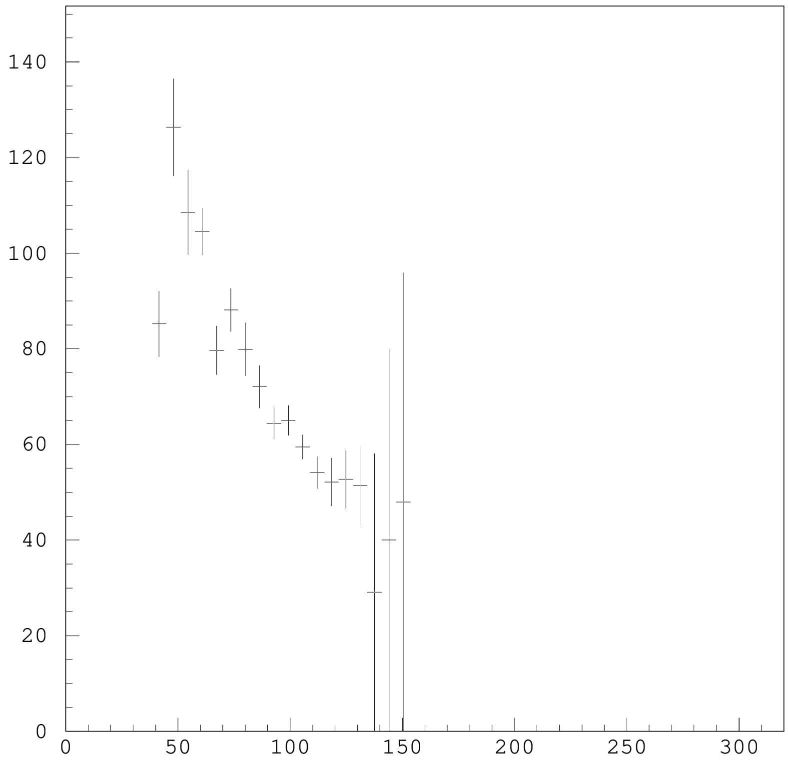

Figure 9: Mean neutron-area energy as a function of PCAL transverse energy in Au-Al collisions.

result of the analysis without using the charged particle veto in the forward scintillators. This is more important at lower E_t (higher UCAL neutron region energy). Note that the statistics at higher UCAL energy here are much improved without the cut.

An interesting cross check, and an interesting measurement itself, is the inverse of the distributions described above: the mean neutron-area energy as a function of PCAL E_t. This is shown for the different targets in Figures 9, 10, 11 and 13. The dependence of the mean forward neutral energy against E_t is more clearly seen in these distributions.

Figure 12 shows the result for the thin Au target, again with and without the scintillator cut. The effect of the cut is very nominal, and consistant

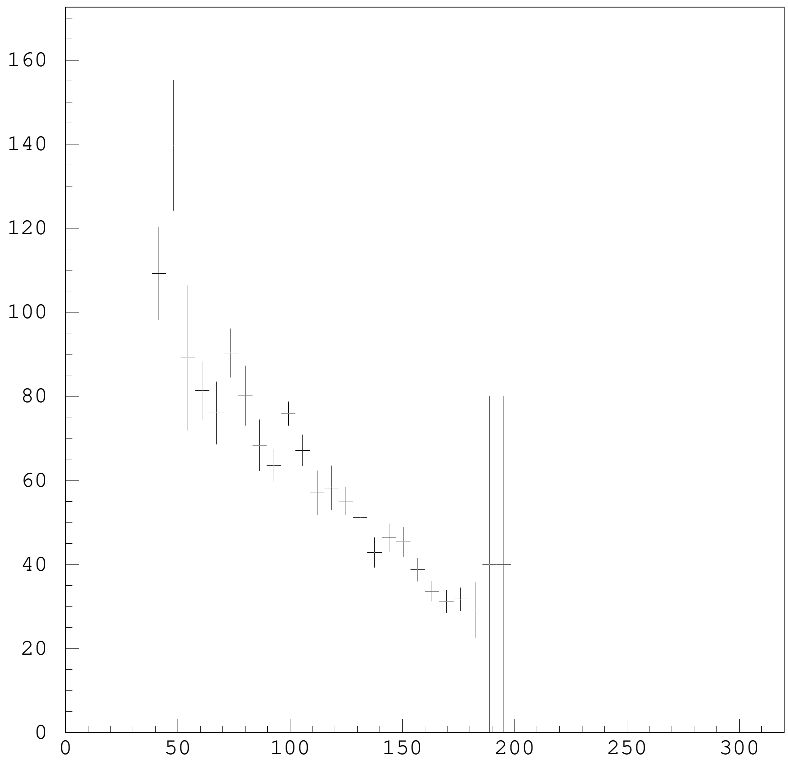

Figure 10: Mean neutron-area energy as a function of PCAL transverse energy in Au-Cu collisions.

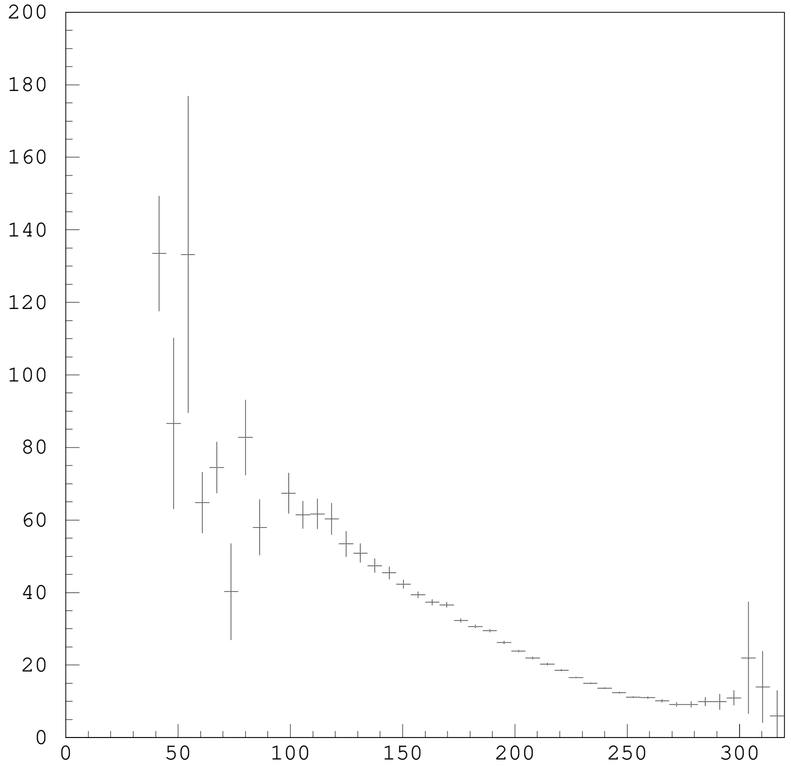

Figure 11: Mean neutron-area energy as a function of PCAL transverse energy for the Au beam incident on the 1% Au target. The mean was formed using a cut on the forward scintillators around the neutron fiducial area, requiring no charge particles, and on the UCAL total energy versus PCAL energy, vetoing on 2-beam particle overlaps.

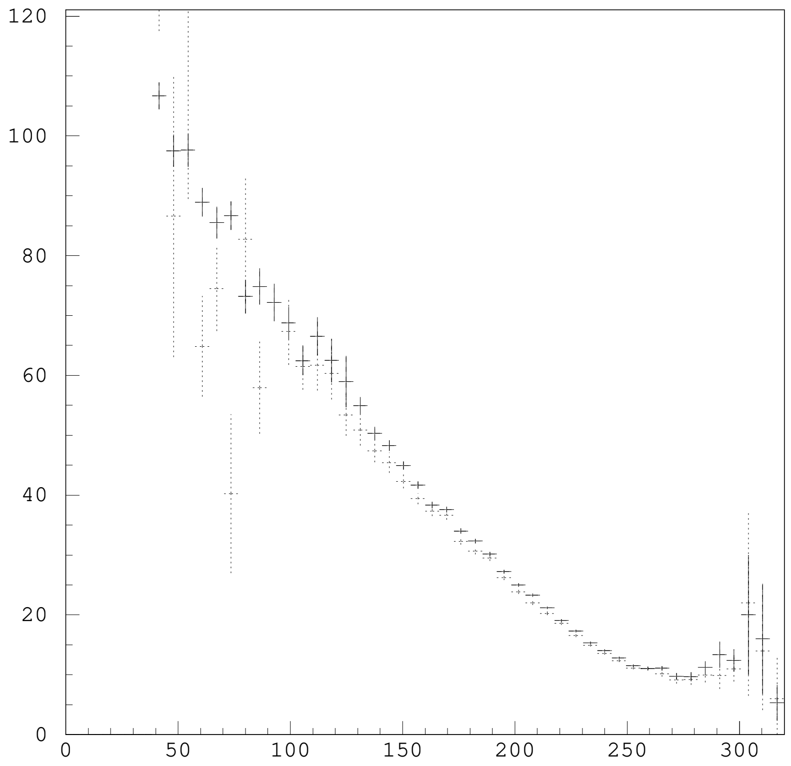

Figure 12: Mean neutron-area energy as a function of PCAL E_t for the Au beam incident on the 1% Au target. The mean was formed NOT using a cut on the forward scintillators around the neutron fiducial area. Also shown is the data with the cut (the dotted curve). The scintillator cut has little effect on the mean measured over E_t. At low E_t this cut has the greatest effect on the statistics of the measurement, presumably due to the copious delta rays arising from nearby beam fragments.

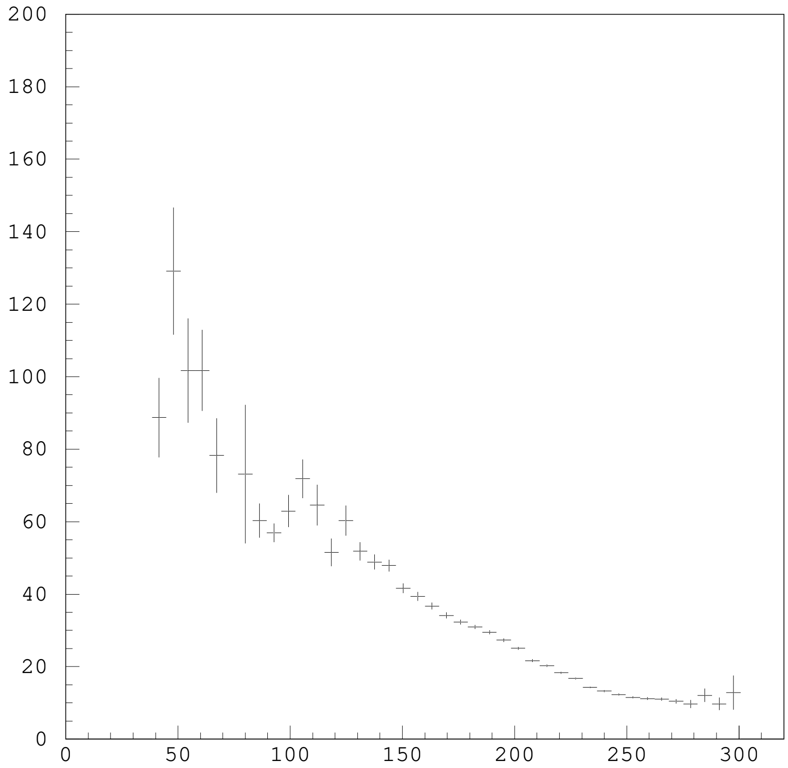

Figure 13: Mean neutron-area energy as a function of PCAL E_t for the Au beam incident on the 1.9% Au target.

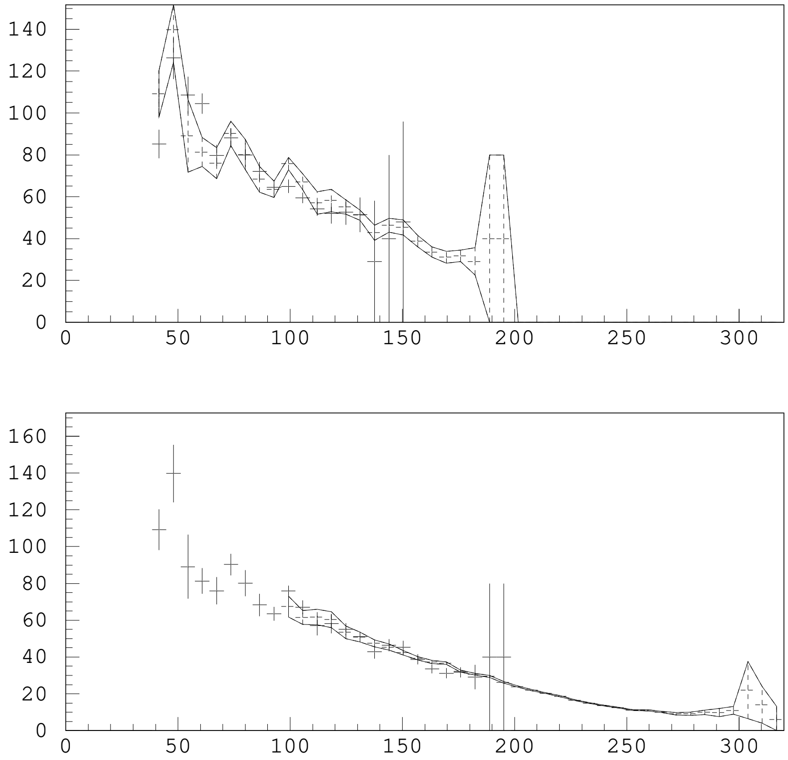

Figure 14: Mean neutron-area energy as a function of PCAL transverse energy for the 3 targets, Al, Cu and Au. The top graph shows the Al and Cu data, the bounded curve being the Cu target data. The lower graph shows the Cu and the 1% Au target data, the bounded curve this time being the Au data. The beam-rapidity neutron multiplicity appears to be primarily determined by the projectile and the collision transverse energy only.

with a delta ray source at low E_t and low-energy secondary pions bent by the analyzing magnet back into the acceptance at high E_t.

In Figure 14 we combine data from the different targets. Note that the mean forward neutron energy as a function of centrality seems independent of target nucleus. Of course the projectile nucleus is the same in all cases. To the extent that the transverse energy is proportional to the number of participants, and the forward neutron energy only dependent on the number of projectile spectators, then it might be expected that for the same number of participants that these different target data would show the same dependency on transverse energy. The lighter targets are not able to provide as many participants of course, so they do not reach the large values of E_t (and the correspondingly small value of neutron total energy).

It is interesting that the thin Au target shows some indication of structure on the tail of the E_t distribution. If this were due to multiple interactions in the target then this would be more obvious in the thicker Au target, yet the opposite seems to be the case.

2.3 Width of the forward neutron-area distribution

We assume for this discussion that the forward energy measured in the neutral region is Gaussian distributed at the UCAL plane, about the undeflected beam line of the experiment. We then measure the width of the 2-dimensional Gaussian distribution as a function of transverse energy, by taking the total of the mean neutral area energy within each PCAL E_t bin for several UCAL stacks within the neutron fiducial region. By plotting this energy as one includes UCAL stacks into the mean energy, starting from the outside, we are effectively evaluating experimentally the integral of the Gaussian as we proceed across the center line. By using a two-dimensional error function to fit the shape of the differential fiducial region, one can fit the width of the neutral area energy distribution.

Figure 15 shows the mean neutral area energy as a function of transverse energy, as one includes more UCAL stacks into the measurement. These data are then divided into 4 PCAL E_t bins, 100-150 GeV, 150-200 GeV, 200-250 GeV and 250-275 GeV, and the curves fit to straight lines within each bin. The total mean area is then found for each curve, for each E_t bin. Figure 16 shows the data for the 4 PCAL E_t bins as well as the fits. Since the fits to the widths are sensitive to the beam undeflected line, and since this

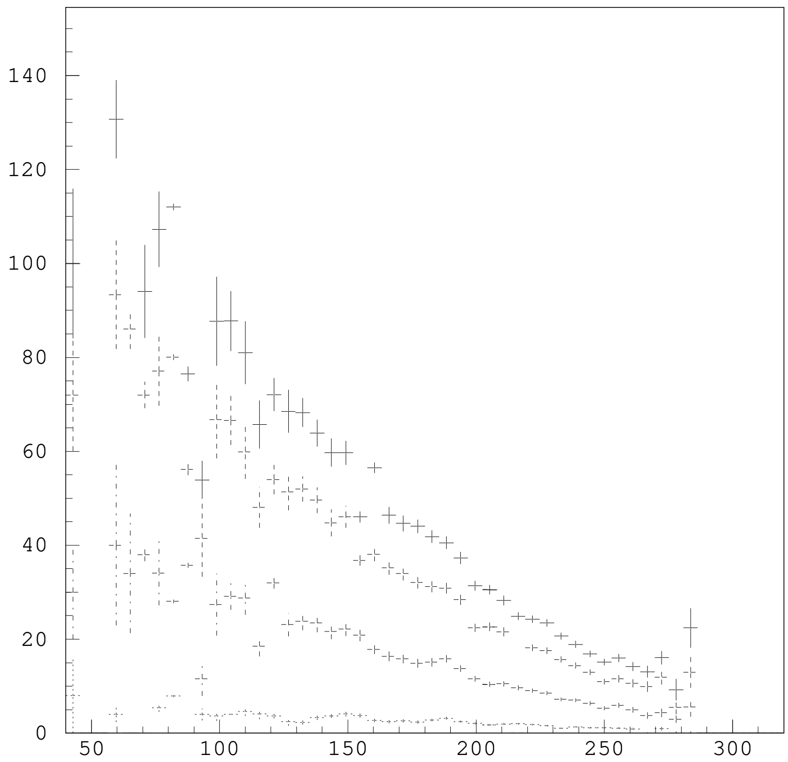

Figure 15: Mean neutron-area energy as a function of PCAL transverse energy for the thin Au target. The lower curve is that measured by UCAL stacks 22-23, the curve above that as measured by stacks 21-23, then 20-23, then 19-23. The undeflected beam line is near the middle of stack 20.

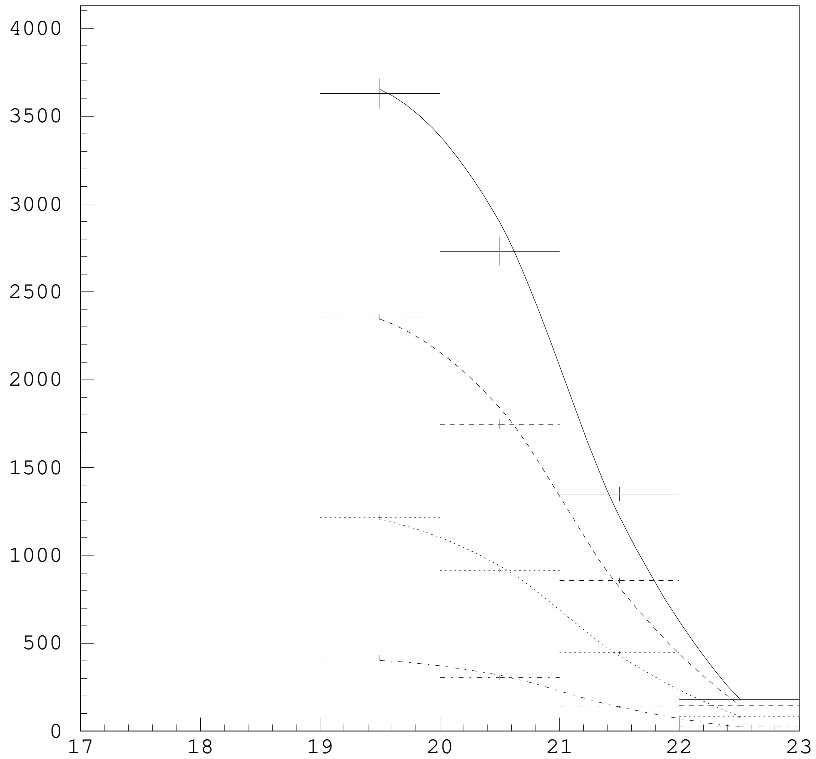

Figure 16: Shown is the rise in the measured neutral area energy as UCAL stacks are added to the measurement, for 4 PCAL E_t bins. The top curve corresponds to PCAL E_t of 100-150 GeV, then 150-200, then 200-250, and the lowest curve to 250-275 GeV. The fits shown then give the corresponding Gaussian widths versus E_t.

actually changes during the AGS spill, we are careful to restrict this center line of the incident beam using the Beam Vertex detector. The data are fit using MINUIT, allowing the vertical scale factor, the centerline position, and the distribution width to all vary, and the error matrix is calculated for the result. The weighted mean of the centerline positions is thus found for the 4 PCAL E_t bins, the smallest error (largest weight) being for the 2 middle E_t bins. The centerline result is checked against the data taken with no magnetic field, and found consistent.

The resulting Gaussian widths are shown in Figure 17. The uncertainty in

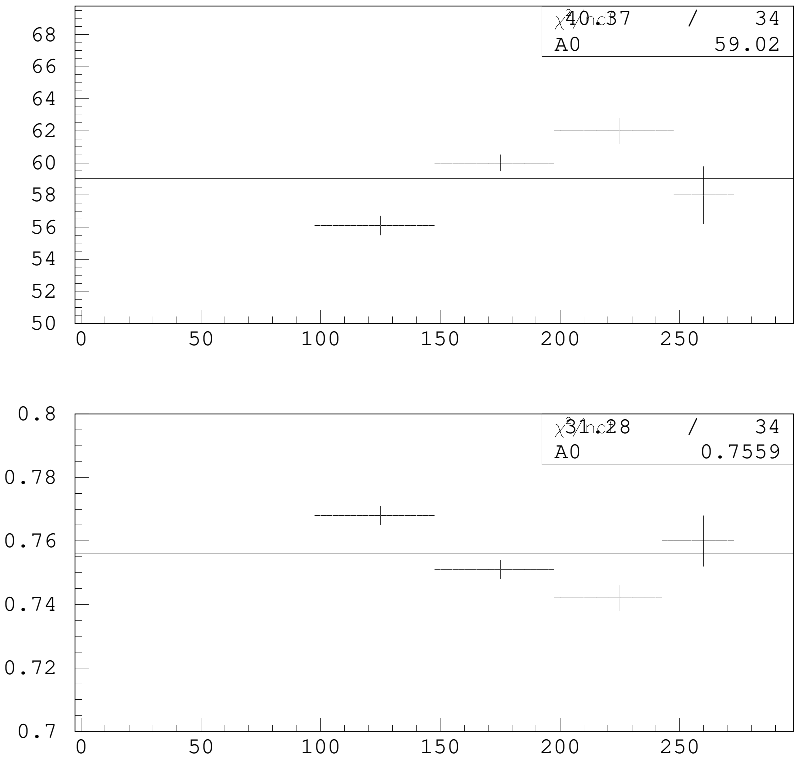

Figure 17: The upper graph shows the 2-dimensional Gaussian widths of the neutral area energy at the UCAL plane, in units of MeV/c, as the effective lateral dispersion in momentum from the target. These are shown for 4 PCAL E_t bins. The errors are those arising from fitting the curves in the previous graph. The lower graph shows the corresponding fraction sampled in our fiducial area The mean fraction is $0.756 \pm .002$.

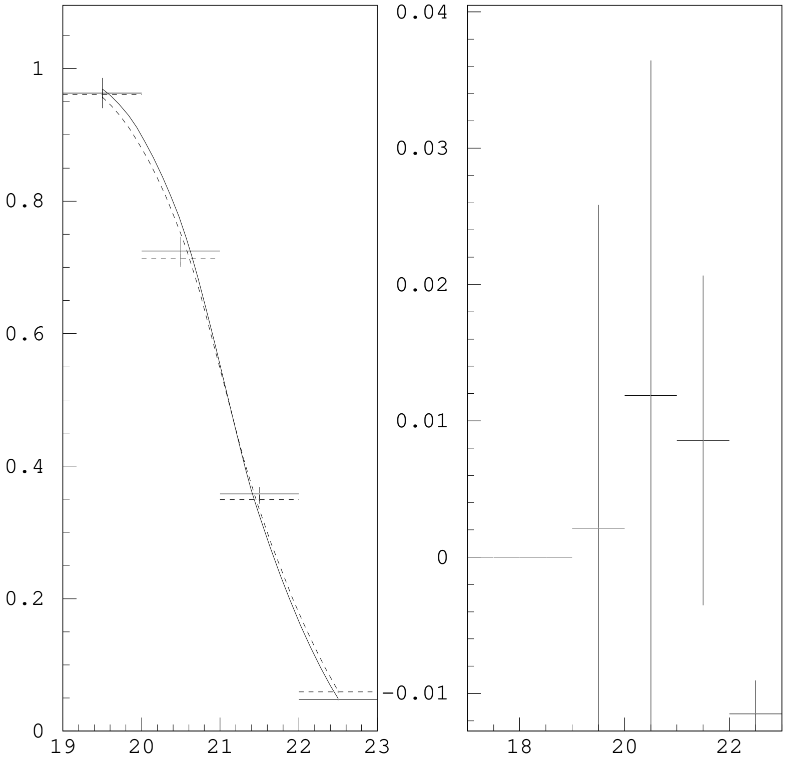

Figure 18: E_t bin 100-150 GeV (solid curve) and 150-200 GeV (dashed curve). The graph on the right shows the difference between the two sets of data, bin-by-bin.

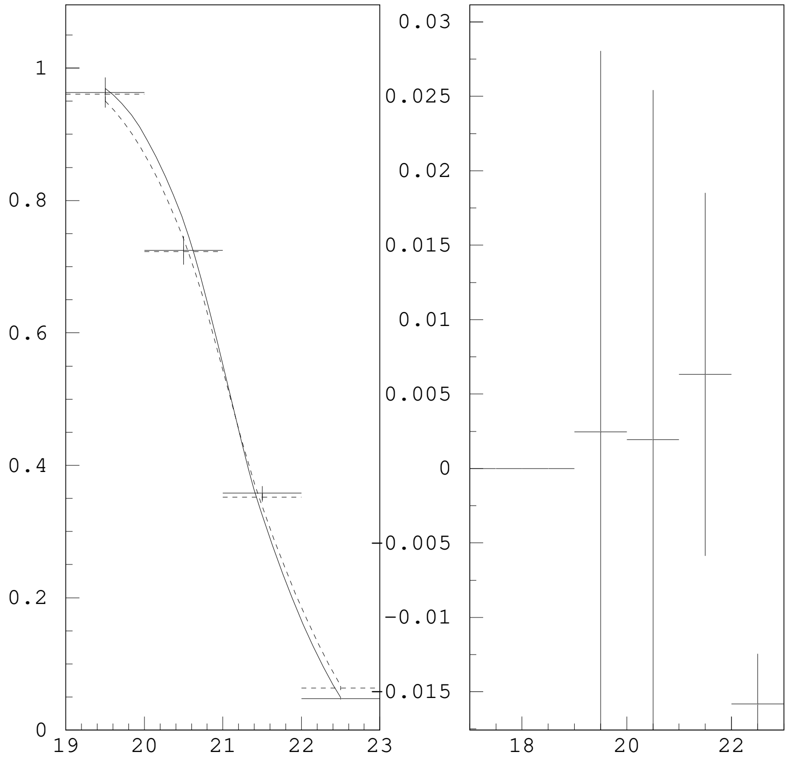

Figure 19: E_t bin 100-150 GeV (solid curve) and 200-250 GeV (dashed curve). The graph on the right shows the difference between the two sets of data, bin-by-bin.

the center line position contributes a vertical systematic error of ≈ 8 percent. The overall shape of the fitted widths as a function of transverse energy is independent of this position to a good approximation. Shown in the lower graph are the corresponding sampling area of the total neutron energy in our fiducial region. The mean is shown in both graphs. For simplicity we will take the normalized sampling area here to be constant with E_t, for later correction of the data. The rise in the width with E_t is not expected in a simple fragmentation model and is not understood.

The significance of this rise is explored in Figures 18 and 19. Shown on the left side graph of each is the normalized curve for the lowest E_t bin (solid line) and the curve the a higher E_t bin. Figure 18 shows the E_t bin from 150-200 GeV (dashed) and Figure 19 shows the bin 200-250 GeV (dashed also). The difference between the two in each case is subtle. The Figures on the right are the differences in the data between each. One sees that the greatest difference between these E_t bins lies in the data point furthest from the experiment center line. In each case the lowest E_t bin is about 3σ lower at this periphery than the higher E_t bins, "pulling" the fitting to a narrower width. The other points nearer the centerline in each case are consistant with a narrower width for the lowest E_t bin, but statistically unconvincing.

2.4 Neutral region Statistics

Naively one might think that the statistics governing the forward neutrons measured would follow a Poisson distribution in any one (small) PCAL E_t bin. For such a statistic, the mean and the variance are equal of course. In Figure 20 is shown the mean normalized to the beam rapidity energy per nucleon for the 1% Au target, and the variance, normalized to the square of the same energy, on the same graph. The two curves are very similar to each other, the variance being close to the mean for any PCAL E_t bin. It is of interest to describe the distibution of neutral-region energy as a function of PCAL E_t. For this, we expect a somewhat more complicated distribution than that given by Poisson statistics.

We would like to choose a statistic that is simple (has a small number of parameters to fit) yet one that might give some physical insight into the spectator model. Let us assume first that the forward neutrons come out of the projectile spectator nucleons. For some PCAL E_t bin that is small, we assume some number of spectators remaining. This isn't true of course, there

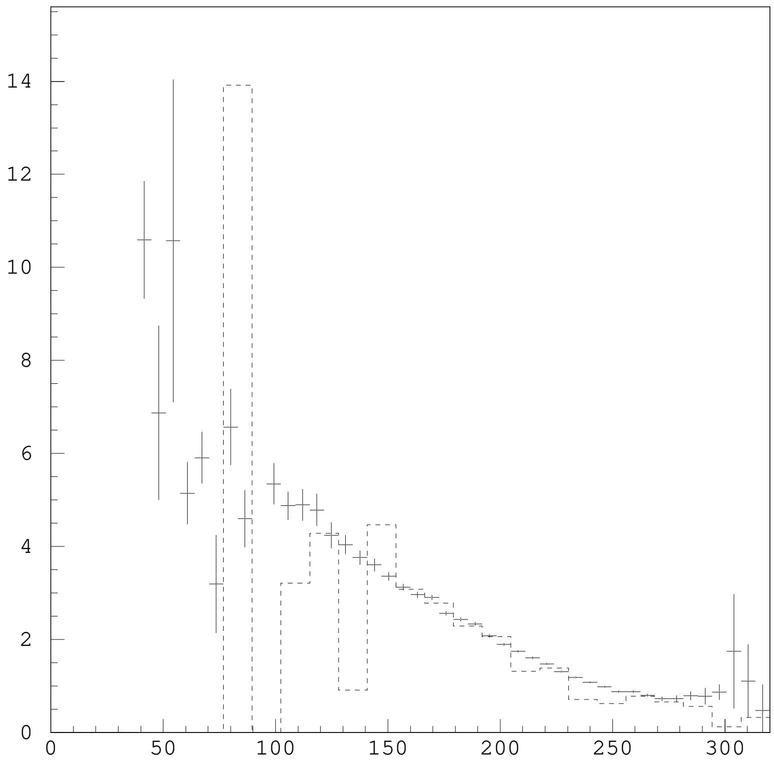

Figure 20: Mean neutron-area energy as a function of PCAL transverse energy for the thin Au target. The mean was normalized to the beam rapidity kinetic energy actually measured by the UCALs for one nucleon, and the variance normalized to the square of that energy. For a Poisson distribution, these two curves would be equal to each other.

are fluctutations in transverse energy such that for any one E_t bin there is also a distribution in the number of participants. However, we would like to try the simple model first, and see if the neutron energy distribution can be fit with a small number of parameters. For some number of spectator nucleons in each E_t bin, N_s, we assume that on average there will be (118 neutrons/197 nucleons)$\times$(N_s) neutrons. (In other words, the fraction of neutrons to the whole nucleus is maintained in the subset, on average.) The appropriate statistic for sampling within a subset of a larger fixed set is the Hypergeometric distribution, which will give a distribution in the number of spectator neutrons for a given E_t bin.

There is then the probability that a spectator neutron will proceed forward without binding to a spectator proton; this probability shall be called p. The number of spectator neutrons actually continuing forward with beam momentum is assumed to follow a binomial distribution, from the number of spectator neutrons given by the previous distribution, with this individual parameter of "success" p. Then there is the probability that a forward neutron falls within our fiducial area. Given the spatial widths of the neutrons from the previous section, (assuming a mean width that is constant with E_t), we know the probability of finding any forward neutron in our fiducial area ($\approx$75%, not the factor of 1/2 naively estimated originally). The fraction of forward neutrons actually sampled then is also assumed to be governed by a binomial distribution, with the parameter of success being the total area of the Gaussian production covered by the fiducial area, p_f. These equations are given explicitly in section 3.

By convoluting these three distributions together, we arrive with a potentially powerful descriptor of the neutron number distribution in any one PCAL E_t bin, with only two free parameters, the number of spectators in the E_t bin, and the probability of the spectator neutron remaining unbound, p. Figure 21 shows the neutral region energy for a mid-E_t and high E_t bin. A fit is also shown about one peak in the upper graph. This fit corresponds to the kinetic energy of one beam-rapidity nucleon, with a resolution of $\approx$ 5 GeV. The actual UCAL resolution on the sum shown is $\approx$ 1/2 this. (The Gaussian tail on the negative side of 0.GeV is consistant with this.) The total energy distribution in our centerline-region is no doubt clouded by neutrons falling near to the edge of the fiducial area. On average, the energy leaking out will be balanced by nearby neutron shower energy leaking in, and to first order cancels out in the mean. In spite of this, we proceed with fitting the neutron

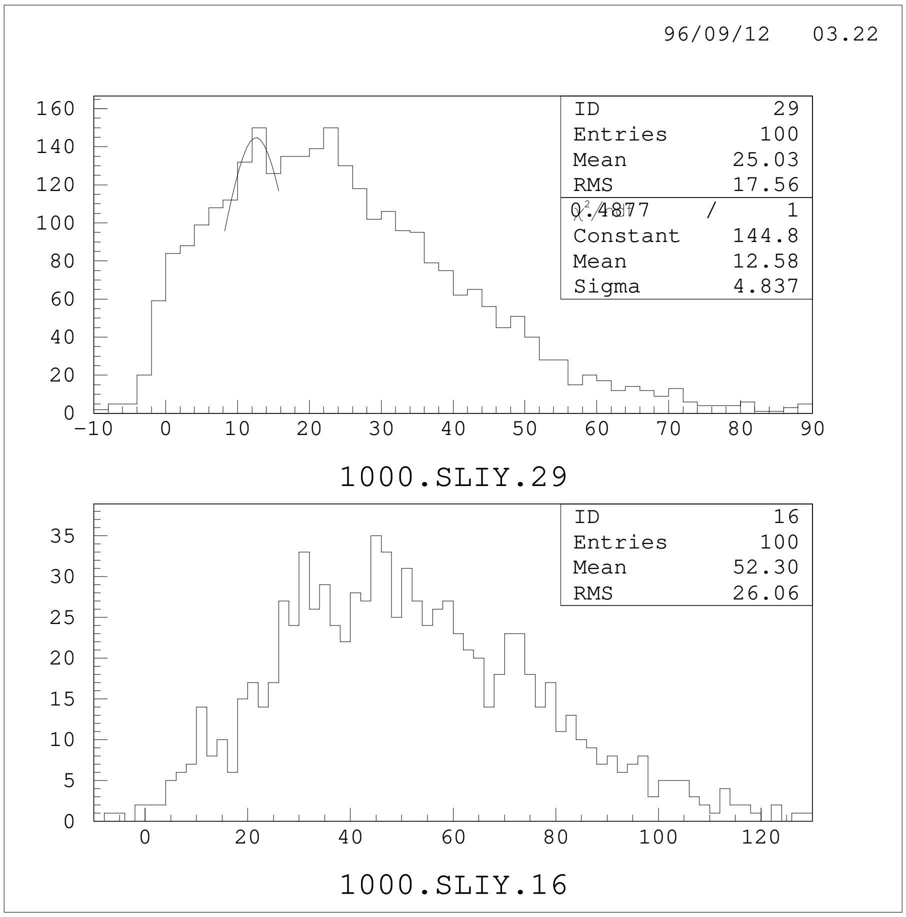

Figure 21: Neutron-area energy for 2 PCAL E_t bins, 130-135 GeV, and 202-207 GeV. The higher E_t shows a beam rapidity peak.

number spectra by simply binning around multiples of beam-rapidity kinetic energy and including an overall scaling factor. One gets fits such as in Figure 22, the PCAL E_t bins being as labelled, for the thin Au target. That the fitting can match the data so well credits the method. Two higher E_t bins are shown in Figure 23.

The parameters determined in the fit are shown in Figure 24. The starting values into MINUIT were not so far from the number of spectators shown in this figure, MINUIT then varying all parameters and converging on a (nearby) solution with the values of p shown. The difficulty is that the mean of the distribution in an E_t bin is highly correlated to both N_s and p. Alternately, one can fix the values of p to be 7.5%, and let MINUIT fit only

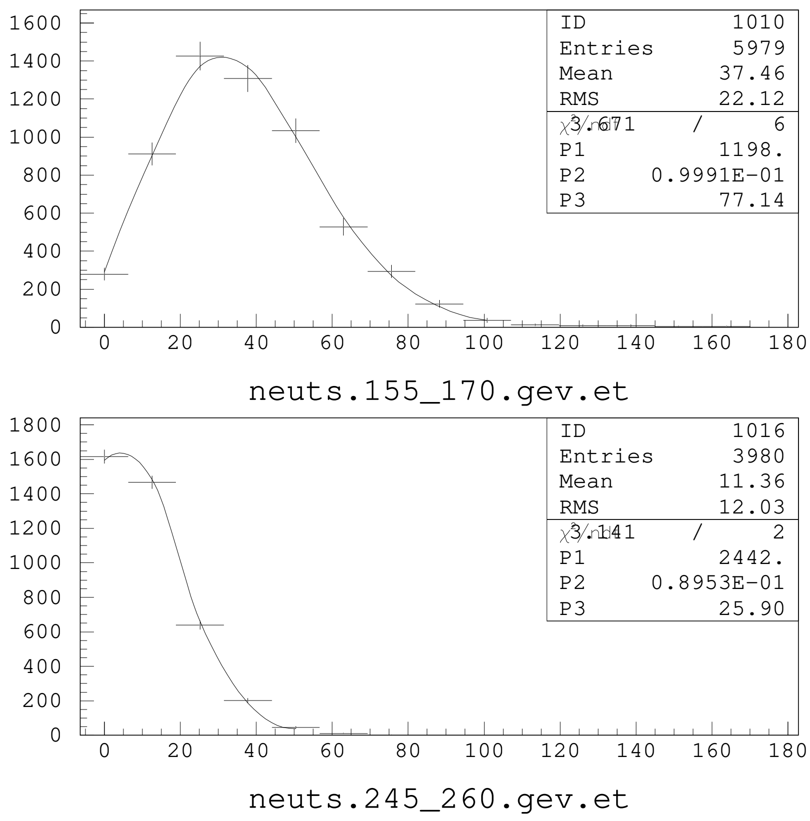

Figure 22: Mean neutron-area energy spectra in bins of beam rapidity energy for two PCAL E_t bins. The model fits well.

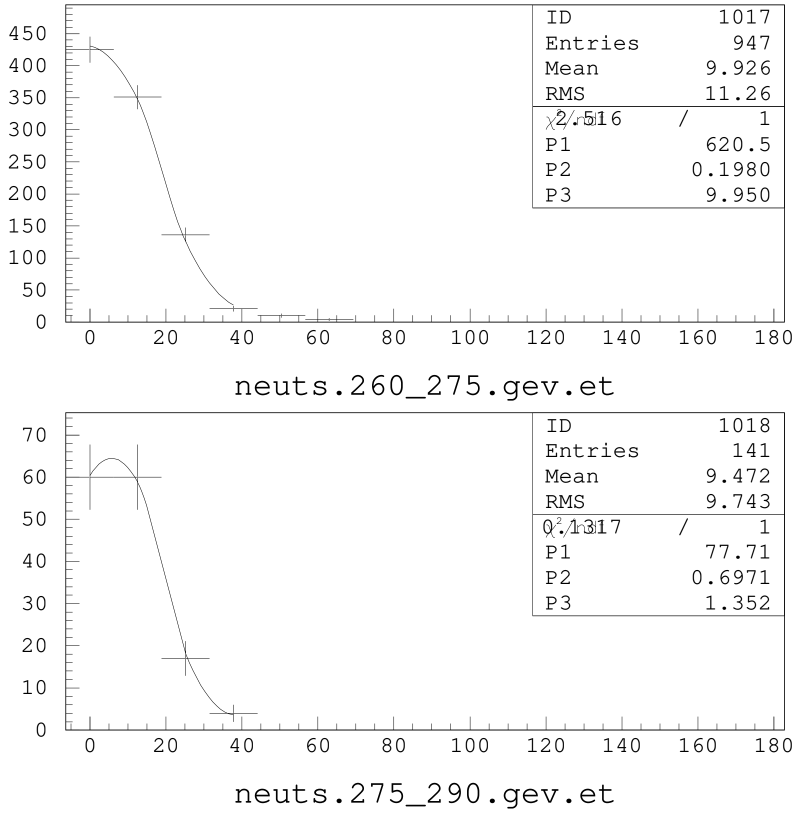

Figure 23: Mean neutron-area energy spectra in bins of beam rapidity energy for the two higher PCAL E_t bins.

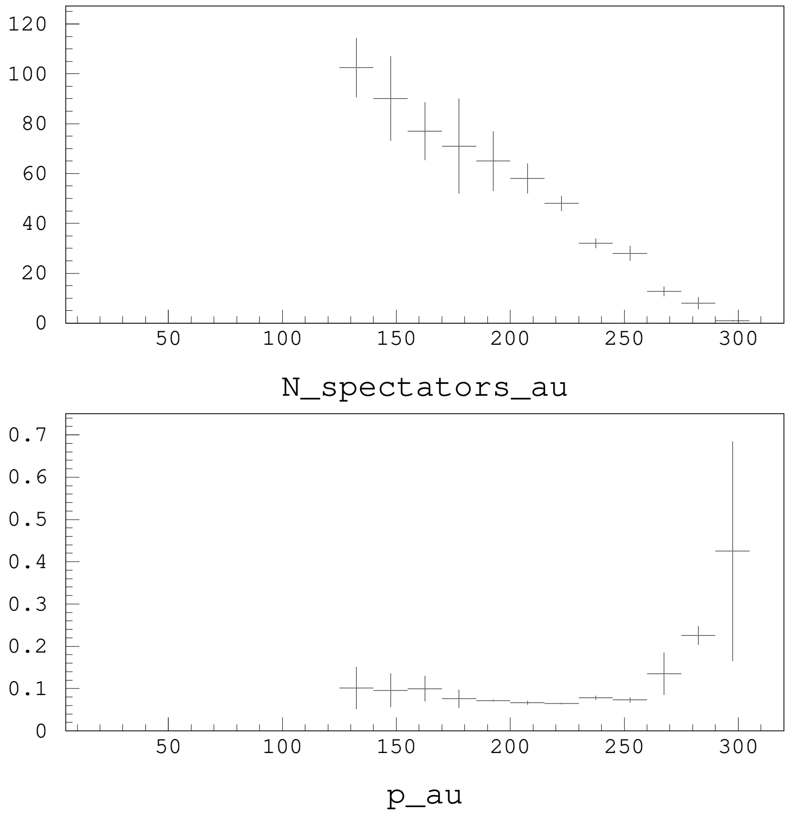

Figure 24: The number of spectators is shown for the thin Au target neutron spectra, as fit by our model as a function of PCAL transverse energy. The corresponding parameter p in the fit is shown in the lower graph.

the value of the number of spectators. The result of this is shown in Figure 25.

It should be argued that the values of p and N_s suitable at a PCAL E_t of $\approx$ 250 GeV should remain constant in bins of still higher E_t. While cutting on higher E_t the actual physics governing the forward neutrons is not changing; the cut effectively selects higher fluctuations in E_t for the same physics sample. See however the lower graph in Figure 25. The χ^2 for the fitting is also shown. The dashed histograms correspond to the fitting which requires the parameter p to remain constant. These χ^2 values are somewhat worse than in the fitting where p is allowed to rise freely. For

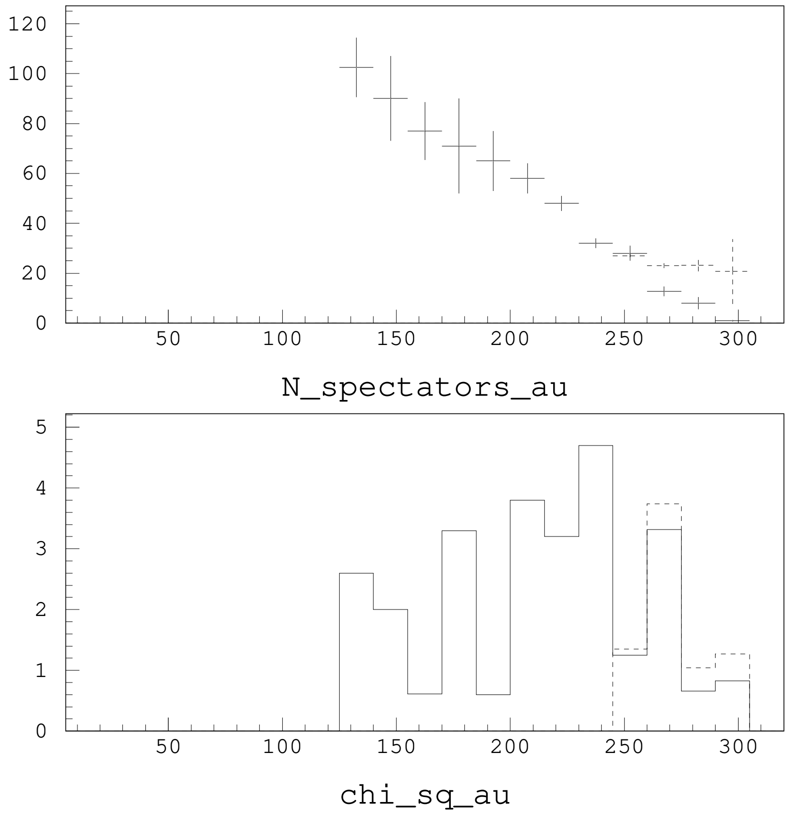

Figure 25: The number of spectators in the Au target fitting of the neutron spectrum, as a function of PCAL transverse energy, where the parameter shown in the previous plot is fixed to be 0.075. Instead of p rising, N_s remains roughly constant on the E_t tail. The lower graph shows the χ^2/d.o.f. for the fits. The dashed histogram corresponds to those fits where p is fixed and N_s rises, at the high E_t tail.

comparison sake, p was allowed to vary with small step size in both cases, into a local χ^2 minima, so that the number of degrees of freedom would technically be the same. If p is considered strictly fixed, then the χ^2/d.o.f. would be correspondingly higher by one less degree of freedom. The highest E_t bin near 300 GeV has very large uncertainties.

One can do the same fitting to a lighter target neutron spectrum. Figure 26 show the best fit for the number of spectators and the parameter p to the neutron spectra, from the Cu target data. No such unusual behaviour at the endpoint of the PCAL E_t spectrum is seen as compared to the Au target data.

2.5 Correlations on the E_t tail

Figure 27 shows the mean energy in 3 UCAL stacks around the region where the beam rapidity protons would be expected to lie. These protons should be centered on UCAL stack 12, and the quantity plotted is the mean summed energy in stacks 10, 11 and 12. The top curve shows the mean for all triggers as a function of E_t. The mid-graph shows the same when requiring that there be no energy in the neutron-region of the UCALs, and the bottom graph when requiring that there be at least one neutron found in the neutron region. The structure on the endpoint of the E_t spectrum on top is clearly correlated to the energy in the neutron region. It may well be that the "bump-like" shape arises from the falling spectrum from the no-neutron case, averaged with that correlated to the neutrons and extending somewhat further in E_t.

Figure 28 shows the same analysis for 4 UCAL stacks, stacks 4, 5, 6 and 7, that are so far away from the beam that no beam-rapidity particles would be expected to fall in this region. This region would sample mostly secondaries from the interaction. The top graph shows the mean summed energy in these stacks, when requiring at least enough energy in the neutron region consistant with at least one neutron. The bottom graph was made requiring no neutral-area energy. A similar correlation to that found in the proton region is seen.

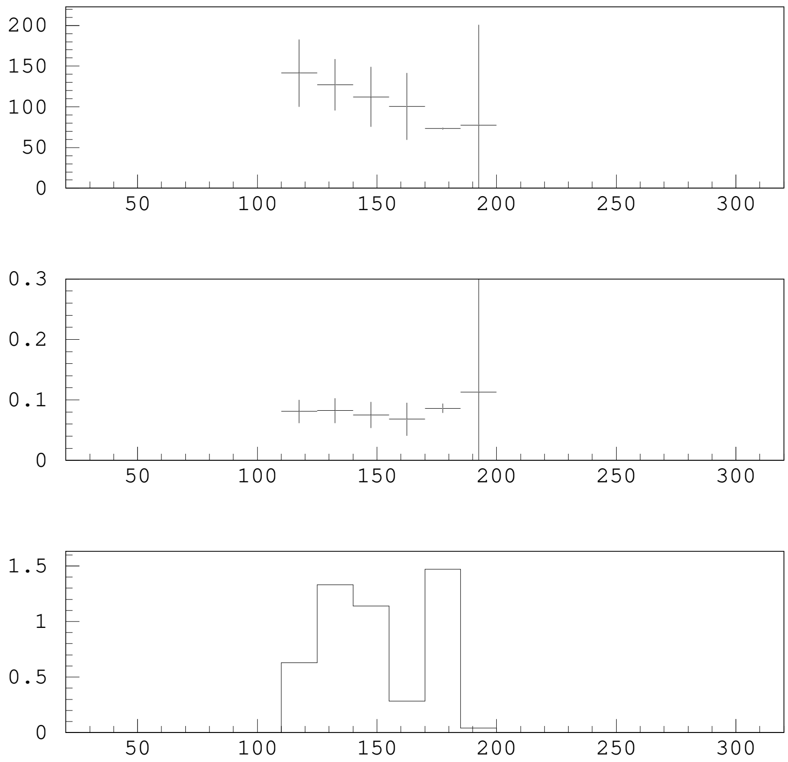

Figure 26: The number of spectators in the Cu target fitting of the neutron spectrum, as a function of PCAL transverse energy is shown in the upper graph, the parameter p in the middle graph. The lower graph shows the χ^2/d.o.f. for the fitting. No unusual change is seen on the E_t tail in the Cu target data, within statistics.

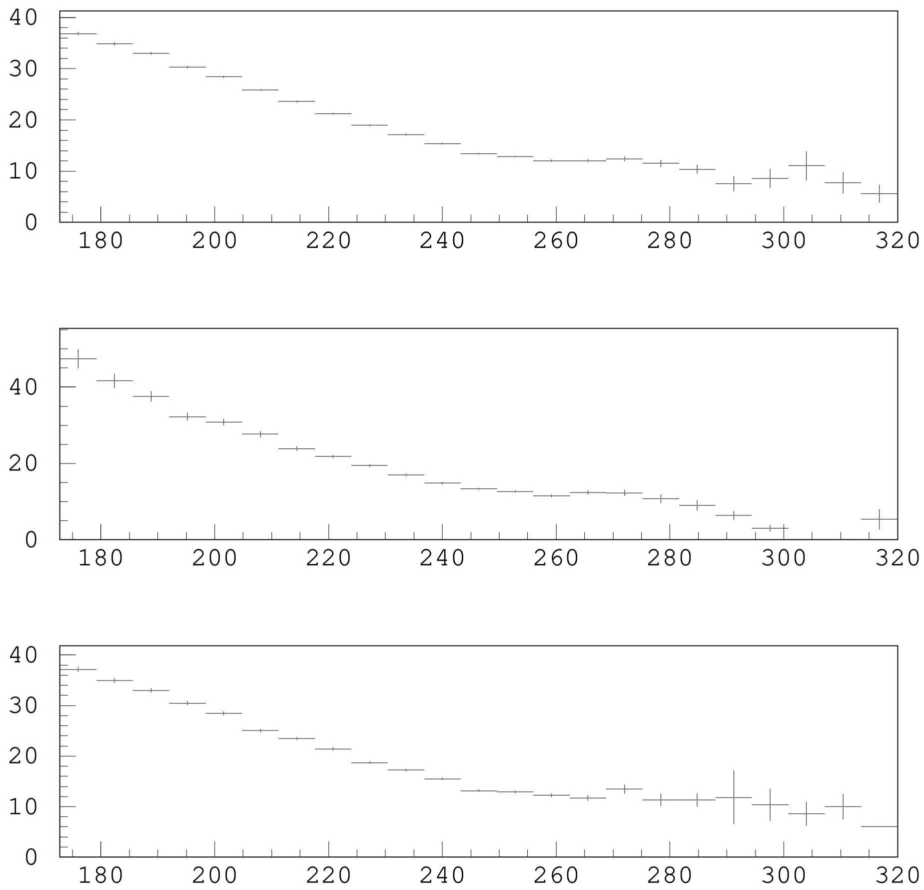

Figure 27: The mean summed energy in the beam-rapidity proton region is shown in the upper graph, the same requiring no neutron region energy in the middle graph. In the bottom graph, energy consistent with at least one neutron is required in the centerline-region, showing a correlation to the proton region at the highest E_t.

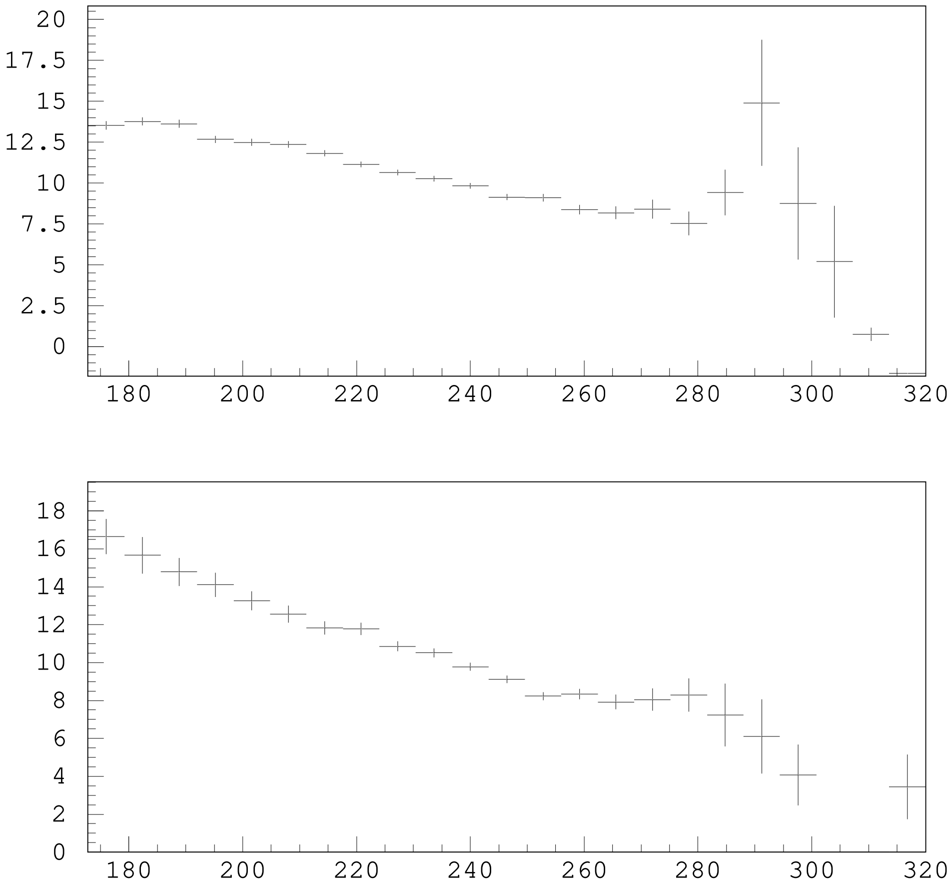

Figure 28: The mean summed energy in a UCAL region that can only be dominated by secondaries is shown. The bottom graph was made requiring no neuton-region energy deposit. In the top graph, energy consistent with at least one neutron is required in the centerline-region, showing a correlation at the highest E_t.

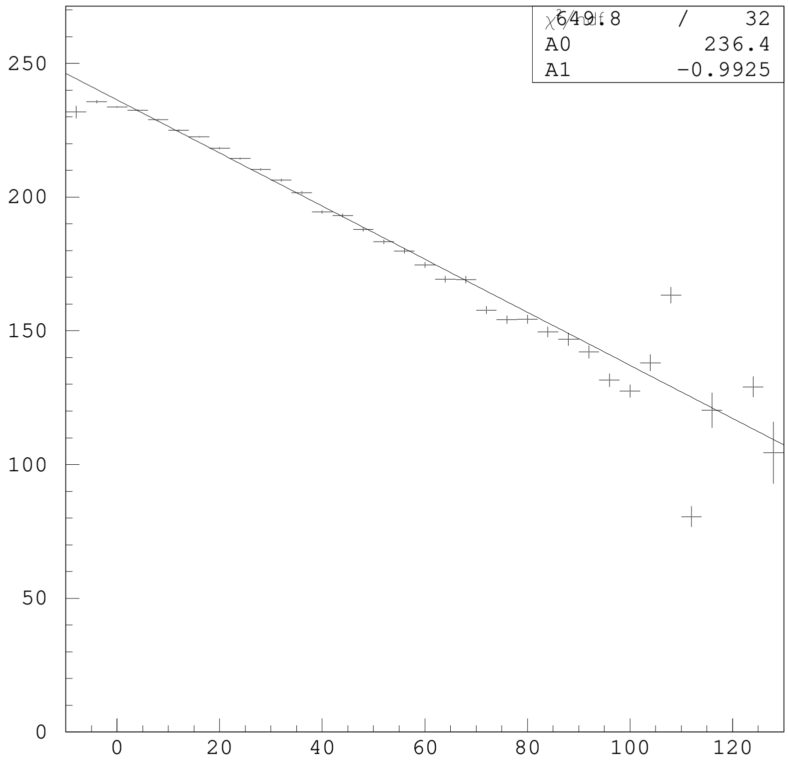

Figure 29: The mean summed energy in a PCAL versus the UCAL neutral-region energy for the 1% Au target, as fit to a line. The parameters of the line are shown. When corrected for the fiducial area of the neutrons measured, the equation of the line becomes $\overline{E_t}$ (GeV) = (-0.993$\times$0.756)E$_n$ + 236.

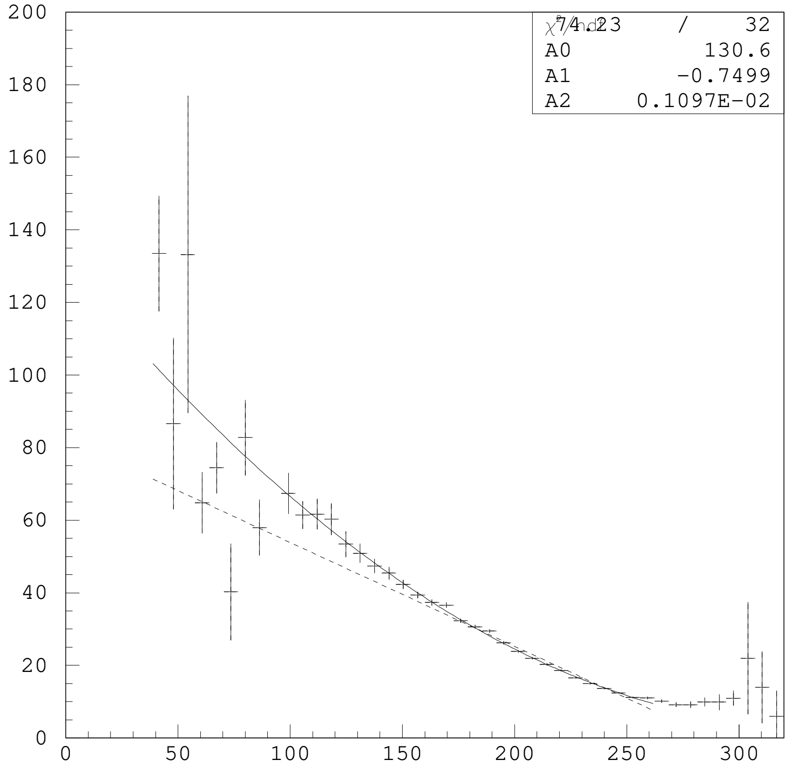

Figure 30: The mean summed energy in a UCAL neutral region versus the PCAL E_t for the 1% Au target data. Shown are fits to a line, and to a parabola. The χ^2/dof for the parabola is 2.3, even over this large range in E_t. When corrected for the fiducial area of the neutrons measured, the equation of the parabola becomes $\overline{E_n}$ (GeV) = 172.4 - 0.99E_t + 0.00145E_t^2.

3 Remarks

The mean transverse energy in Au-Au collisions as a function of the forward neutrally-charged energy has been studied, showing a linear dependence of E_t over a wide range of such energy. The corresponding small widths to the E_t distribution (from ≈25% at more peripheral impact parameters down to less than 10% at small impact parameter indicate that such a forward measurement at RHIC could be useful for event characterization. This dependence is shown as a fit to a straight line in Figure 29, although over a restricted region of the forward neutron energy. This fit, corrected for fiducial area, is given in Equation (1).

$$\overline{E_t}(GeV) = -0.75E_n + 236 \quad (0 \leq E_n \leq 160GeV) \tag{1}$$

$$\overline{E_n}(GeV) = 172.4 - 0.99E_t + 0.00145E_t^2 \quad (0 \leq E_t \leq 250GeV) \tag{2}$$

A similar dependence is seen in the mean forward neutral-area energy as a function of E_t. Shown in Figure 30 is the thin Au target data fit to a line, and to a parabola. The second order polynomial is seen to fit much better. This fit, corrected to fiducial area, is given by Equation (2). The reader might be tempted to normalize to the E_n measured for one beam rapidity nucleon, 12.6 GeV. At very high E_t the linear dependence fails, and the neutron-area energy plateaus-out. Such behaviour is usually seen as a result of cutting on a parameter with large fluctuations, here E_t, on the endpoint of the distribution where it is no longer indicative of a changing event topology. The tantalizing "bump" in the for the mean forward neutron-area energy in the thin Au target data led us to explore this more fully.

The statistical distribution of neutrons for a given centrality of collision, and better yet, as over a range of impact parameters, is an interesting distribution to find. By forming such a distribution as a function of parameters directly related to the spectator model, one can get some insight into the individual nucleon dynamics. Further, such a statistical distribution, if found to apply well over a wide range of E_t, can form a test of the physics changes that are or are not taking place at the endpoint of the E_t spectrum. Such a statistic was found.

Equation (3) is that of a hypergeometric distribution, where N_A= atomic number, p_0= fraction of neutrons in nucleus, N_s= mean number of spectators in some E_t bin, and n the number of neutrons in the spectators subgroup. Equation (4) is a binomial distribution, where p=probability of an initial-state neutron continuing forward through the collision, unbound, and m the number of forward neutrons Equation (5) is also a binomial, representing the fraction of forward neutrons actually sampled in our measurement, p_f being the sampling fraction.

$$P(n) = \frac{\begin{pmatrix} N_A p_0 \\ n \end{pmatrix} \begin{pmatrix} N_A(1. - p_0) \\ N_s - n \end{pmatrix}}{\begin{pmatrix} N_A \\ N_s \end{pmatrix}} \tag{3}$$

$$P(m) = \begin{pmatrix} n \\ n - m \end{pmatrix} (1 - p)^{n-m} p^m \tag{4}$$

$$P(k) = \begin{pmatrix} m \\ m - k \end{pmatrix} (1 - p_f)^{m-k} p_f^k \tag{5}$$

$$\begin{pmatrix} N \\ n \end{pmatrix} = \frac{N!}{n!(N-n)!} \tag{6}$$

$$P_p^{N_s}(k) = \sum_{n=k}^{N_A} P(n) \sum_{m=k}^{n} P(m)P(k) \tag{7}$$

The probability of observing k neutrons is given by Equation (7), for the 2 parameters p and N_s. The number of spectators was fixed to the total number of baryons at E_t=0, and then assumed to depend linearly on E_t. The best parameter p was then found from this number of spectators. The neutron spectra have a dependence on E_t through the dependence of N_s on E_t, given by Equation (8).

$$N_s = -0.696 E_t + 197 \quad (p = 0.0749) \tag{8}$$

These fit the data best at the E_t 'plateau', failing at very high E_t. At low E_t the measurement was confounded by the MT target subtraction. This fit, while striving to be physical, is only intended as a useful paradigm for generating such spectra, and is not to be construed as a particular model.

If in fact the physics governing the event topology is no longer changing one moves higher in E_t in the region of this "bump", then the parameters in this statistical distribution should remain constant, or at least predicatably behaved, above a certain E_t. In fact in the Cu target data such was the case. In the Au-Au data, the χ^2 test was used to show that this was probably not the case.

The "extra" neutrons possibly seen above a certain E_t in the Au-Au collisions are found to be correlated with the energy in the beam-rapidity proton region of the UCALs. There was also a correlation found with the region in the UCALs so far away from the beam line that it would have to be dominated by secondaries from the collision. Furthermore, when dividing events between those with neutrons and those without, the beam-rapidity proton region showed that its own mean energy consists of one distribution that is flat, with another (with somewhat better statistics) that is linearly falling. The combination of the two seems to give rise to a "bump". It is possible that this "bump" is simply an indicator of multiple interactions in the target, giving extra E_t for some production of forward neutron energy actually consistant with a lower E_t. Of course, if this is so then the parameter p in the fitted distribution would be expected to remain constant, while the number of spectators only would change. The χ^2 test indicates otherwise. Also, this effect is less clearly seen in the thicker Au target data, instead of more clearly seen should it arise solely from multiple interactions.

One possible explanation is that as the projectile nucleus aligns itself with the target nucleus, that there is a corona effect on the periphery similar to an incomplete eclipse of the sun when the moon subtends a slightly smaller solid angle as viewed from earth. This allows an unexpected number of initial state projectile nucleons through the "fuzzy" periphery of the target. By the same argument, those projectile nucleons on the periphery that do interact with nucleons in the target will produce secondaries that themselves will be more likely to pass through the "fuzzy" periphery of the target, than if they were produced by a more central projectile nucleon.

4 Acknowledgements

We gratefully acknowledge those in E877 who aided this set of special runs, especially Wen-Chen Chang who refurbished the UCAL modules in the neutral region, and Johannes Wessels, who oversaw the shuffling of these modules into optimal order. We also acknowledge Helio Takai for the many fruitful

discussions during the analysis.

References

[1] J. Barrette et al. (E814 Collaboration), Phys. Rev. **C45**, 819 (1992).

[2] T. Akesson et al. (AFS Collaboration), NIM **A241**, 17 (1985).

[3] T. Akesson et al. (NA34 Collaboration), NIM **A262**, 243 (1987).

[4] M. Fatyga, D. Makowiecki, and W.J. Llope, NIM **A284**, 323 (1989).